Applied Ocean Research 148 (2024) 103948

Contents lists available at ScienceDirect

Applied Ocean Research

journal homepage: www.elsevier.com/locate/apor

Research paper

Assessing the importance of sediment characterization on seabed embedment predictions of cylindrical objects

Saurav Shrestha [a,b,*], Nina Stark [a,b], Brendan Green [a,c], Dan Stilwell [d], Mingyu Kim [d]

[a] Charles E. Via, Jr. Department of Civil and Environmental Engineering, Virginia Tech, 750 Drillfield Drive, Blacksburg, VA 24061, USA
[b] Department of Civil and Coastal Engineering, Engineering School of Sustainable Infrastructure and Environment (ESSIE), University of Florida, 1949 Stadium Road, Gainesville, FL 32611, USA
[c] American Geotechnical and Environmental Services, Inc., 901 East Eighth Ave, Suite 111 King of Prussia, PA 19428, USA
[d] Bradley Department of Electrical and Computer Engineering, Virginia Tech, 453 Whittemore Hall, Blacksburg, VA 24061, USA

ARTICLE INFO

Keywords:
Seabed characterization
Geotechnical properties
Object embedment prediction
Probabilistic prediction

ABSTRACT

The prediction of object embedment into the seabed is important for the deployment and efficacy of submerged sensors and sensor networks, as well as for other applications such as unexploded ordnance risk assessment, subaquatic search and rescue efforts, or anchors and moorings. The embedment of objects into the seabed during placement depends on the strength parameters of the seabed sediment. However, a detailed characterization of seabed strength can be complex and costly since quality seabed samples and/or in situ testing are required. This study evaluates the importance of a detailed geotechnical seabed sediment characterization over seabed classification from geoacoustic surveying or accepting unknown seabed conditions for the prediction of seabed embedment of cylindrical objects. Monte Carlo simulation was applied to model the uncertainty of sediment strength parameters. The results suggest that prior knowledge of the general sediment type (e.g., fine-grained versus coarse-grained as determined from side scan sonar imaging) significantly improves the precision of the embedment predictions over unknown conditions, reducing the coefficient of variation (*CV*) in prediction of percent embedment (*PE*) by about 50 % to 65 %. Performing a detailed geotechnical testing of sediment strength represented a further improvement by 15 % to 35 % over the knowledge of sediment type. Both the mean and standard deviation of *PE* in fine-grained sediments are at least about 3 times the values for coarse-grained sediments indicating a wider distribution of *PE* with deeper embedment for cohesive fine-grained soils. The embedment behavior is a function of the method of deployment (free fall with a certain speed versus placement with no speed) in stiff cohesive sediments but is less relevant in soft sediments since *PE* values are always greater than 100 % (i.e., full embedment). Similarly, in cohesionless sediments, *PE* is always less than 50 %.

1. Introduction

Comprehensive geotechnical characterization of seabed sediments can be a complex and costly task (Lu et al., 2020). Associated challenges, including logistics and budget, become more pronounced when numerous locations or large areas need to be investigated (Stark et al., 2022). Adding to the issue, environmental and seabed conditions can exhibit significant variability from one location to another and may even change over time, as highlighted by Chen et al. (2021). While a thorough geotechnical investigation is undoubtedly advantageous for accurate planning, design, and management of seabed engineering tasks, various factors, such as traffic, environmental conditions, urgency for deployment, costs, and access restrictions, can represent an obstacle to such in-depth studies. However, data needs and information accuracy needs may also vary for different engineering and site investigation targets, and thus, a quantitative assessment of uncertainty and possibly impacts on design, planning, and decision making that may result from different tiers of seabed site investigation, can assist with optimizing site investigation for specific engineering problems. In this study, three tiers of seabed site investigation (no seabed sediment information, knowledge of general sediment type, and a detailed geotechnical investigation) are investigated for the problem of seabed embedment of a cylindric object. The prediction of object embedment into the seabed is important for the deployment and efficacy of submerged sensors and

* Corresponding author at: Department of Civil and Coastal Engineering, Engineering School of Sustainable Infrastructure and Environment (ESSIE), University of Florida, 1949 Stadium Road, Gainesville, FL 32611, USA.
E-mail address: shresthasaurav@ufl.edu (S. Shrestha).

https://doi.org/10.1016/j.apor.2024.103948
Received 5 October 2023; Received in revised form 12 January 2024; Accepted 1 March 2024
Available online 29 April 2024

sensor networks, as well as for other applications such as unexploded ordnance risk assessment, subaquatic search and rescue efforts, or anchors and moorings. For example, the performance of sensors or mooring devices placed on the seabed may be directly related to their seabed embedment depth with many sensors suffering performance loss from embedment and mooring anchors typically gaining in performance from embedment.

Three scenarios of "seabed characterization" are considered: no seabed information are available (in this case being either cohesive fine-grained sediment or non-cohesive sandy sediment); a reliable seabed classification, i.e., cohesive fine-grained versus non- cohesive sand (from here on referred to as cohesive and cohesionless), is available, as could possibly be determined from geoacoustic surveying or from detailed geological maps; and detailed geotechnical measurements of sediment strength to the sediment depth of interest are available. This study includes embedment with time from consolidation but not from active sediment dynamics (e.g., scour or bedform migration).

Extensive research has been conducted to predict the embedment of UXOs (Catano-Lopera et al., 2007; Friedrichs et al., 2016; 2018; Rennie et al., 2017). However, these studies focus almost exclusively on burial due to hydrodynamic and sediment dynamic processes such as scour, and do not focus on embedment during placement. Additionally, most of these studies (other than Rennie et al., 2017) take a deterministic approach and do not consider uncertainty in the governing environmental parameters or available information. Research has also been conducted on the embedment of seabed pipelines (Gourvenec and White, 2010; Gao et al., 2013; Wu et al., 2021). However, in these studies, the pipelines are often assumed to be installed to a certain depth before settlements are computed. Like the UXO burial studies, the governing environmental parameters are typically modeled without consideration for uncertainty in the variables. White and Cathie (2010) showed that the uncertainty in embedment and the subsequent lateral breakout resistance of pipelines can be quantified by applying theoretical pipe- soil interaction solutions in a Monte Carlo analysis. Independent distributions of remolded and reconsolidated strengths were used in theoretical calculations to compute uncertainties in embedment and breakout resistance. There has been extensive research on the embedment of anchors. Experimental studies through centrifuge model testing (O'Loughlin et al., 2004; Richardson et al., 2006) and numerical modeling (Sagrilo et al., 2010) conducted on the pullout capacity of dynamically penetrating anchors indicated that the anchor holding capacity can be determined with high precision, provided that the embedment was accurately predicted. However, the predicted embedment in these studies is assuming accurate predetermined values of soil strength. Another study by Li et al. (2021) predicted the penetration depth of anchors using Young's formula (Young, 1997), but the soil strength, which is represented by a single deterministic value, is unable to predict the penetration depth of anchors at high precision. It should be noted that most of these studies assume that the sediment properties are accurately known, which may not be the case for many applications for a variety of reasons.

Geotechnical site characterization in offshore environments can be challenging and time-consuming. Cone penetration testing (CPT) is the most common technique for evaluating soil conditions in coastal and offshore areas in situ where a cone-shaped penetrometer is pushed into the ground at a fixed rate of 2 cm/s using a rod of the same diameter (Lunne, 2012). Commonly derived parameters are undrained shear strength for fine-grained soils, and relative density and friction angles for coarse-grained soils (Robertson, 2010). Free-fall penetrometers (FFPs) have recently been added to the toolbox of offshore geotechnical engineering as they provide a cost-effective and rapid means of evaluating the strength characteristics of seabed sediments (Osler et al., 2006). These devices aim to derive similar geotechnical properties as CPT, with undrained shear strength commonly derived for fine-grained soils (Aubeny and Shi, 2006). In recent years, FFPs have been used to assess relative density and friction angles in sandy nearshore environments (Albatal et al., 2020) and to estimate the coefficient of consolidation of fine-grained nearshore and estuarine sediments (Mumtaz and Stark, 2020). FFPs may present a more time- and financially efficient method for geotechnical evaluations of near-surface sediments in the seabed. However, it should be noted that these instruments still represent point measurements of seafloors sediments. Soil samples collected using sampling and coring devices can be processed in the laboratory to obtain a wide range of geotechnical properties, but the collection of undisturbed and quality samples suitable for reliable testing can be difficult to nearly impossible at sites (Karlsrud and Hernandez-Martinez, 2013).

Geophysical techniques measure variations in the physical characteristics of the seabed (Shendi, 2007). Side scan sonar and backscatter intensity maps derived from multi-beam echo sounding have successfully been applied to map seabed surface sediment types (Shang et al., 2019). Sub-bottom profiling techniques are commonly used to scan into the seabed and depict seabed stratigraphy in the upper meters to tens of meters of the seabed. Geotechnical properties of seabed sediment layers have been assigned to sediment deposits using geoacoustic methods combined with geotechnical testing (Chen et al., 2021). Also, initial attempts have been made towards estimating geotechnical properties directly from geoacoustic surveying (Jaber et al., 2021). However, to-date, while geoacoustic surveying allows confident mapping of general sediment types, direct estimates of geotechnical properties are not considered reliable without complementary geotechnical testing in situ or in the laboratory.

In summary, comprehensive geotechnical and geophysical surveys of the seabed provide invaluable insights for predicting object embedment, and generally, for seabed site investigation for offshore engineering problems. Yet, challenges arise from the time- and cost-intensive nature of offshore data collection, coupled with issues related to sample quality, measurement accuracy, and instrument deployment feasibility. This complexity necessitates an optimized approach to seabed characterization, acknowledging factors often beyond the control of survey planners and decision-makers. Understanding uncertainties and their impacts of different site investigation methods can assist with optimizing site investigation. The goal of this study is to develop a probabilistic model to predict the embedment of finite-length cylindrical objects deployed on the seabed via placement or freefall. A Monte Carlo simulation is developed to model the uncertainty in the governing sediment strength parameters and to yield stochastic predictions of embedment. This model is then used to determine how knowledge of sediment conditions prior to deployment (represented by three tiers: no seabed sediment data; sediment type is known as cohesive or non-cohesive, i.e., sand or mud; geotechnical data was collected at instrument accuracy) affects the precision of embedment predictions to assess the importance of different data products for the investigated scenarios. The readers are advised not to be confused with words 'sediment' and 'soil', as they are used interchangeably in this paper.

2. Methods

Embedment is assumed to be controlled by two main mechanisms: embedment due to shear failure of the seabed sediment and embedment due to consolidation settlement over time (Simpson et al., 1974). For the purposes of this study, burial due to sediment dynamics (i.e. scour, migrating bedforms, liquefaction) is not considered.

2.1. Deployment methods

Three types of object deployment methods are investigated: placed on the seafloor by winch or divers (i.e., no impact forces), freefall in a vertical orientation (vertical fall), and freefall in a horizontal orientation (horizontal fall) from some height above the seabed (Fig. 1). It is understood that the freefall is idealized, and a cylindrical object would easily start tumbling (Inman and Jenkins, 2002). However, the two

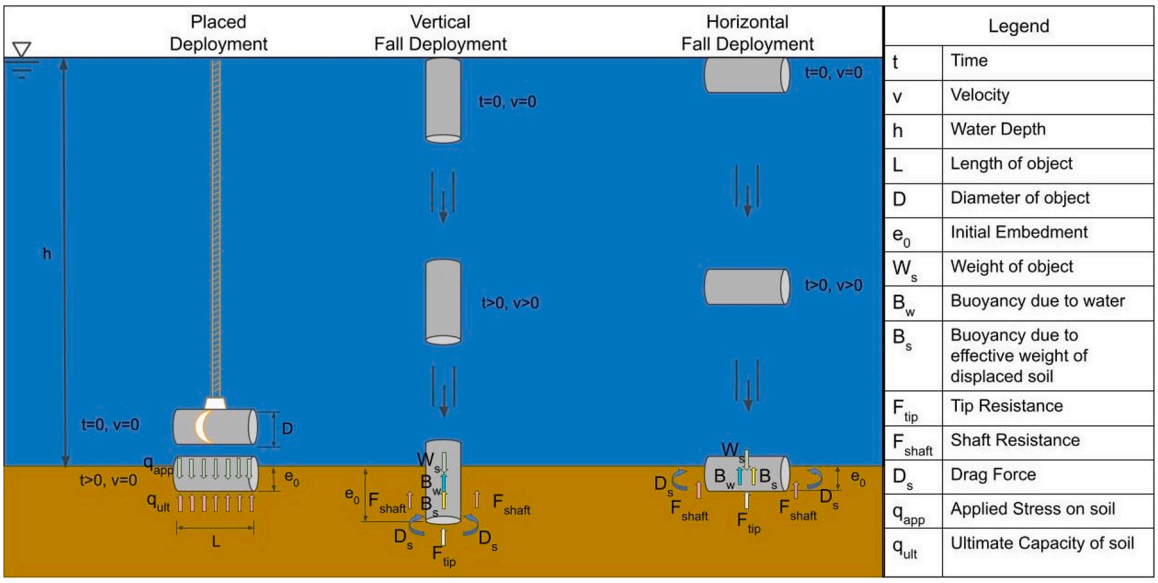

Fig. 1. Schematic representation of the three deployment methods: placed (left), vertical fall (center) and horizontal fall (right). The legend column on the rightmost part of the figure denotes the symbols and their representations.

idealized freefalls are considered here for a representative range of terminal velocity and projected impact areas. The computation of embedment for the two freefall cases is performed using the same set of equations except for the minor difference in usage of geometrical parameters in the equations. Hence, both the freefall cases are discussed within the same section.

2.1.1. Placed deployment

When an object is placed gently on the seabed with close to zero velocity, the buoyant weight of the cylinder ($W_s^{'}$) acts downward on the seabed sediment. $W_s^{'}$ is then resisted by the bearing capacity of the sediment (q_{ult}) and the cylinder will sink into the sediment until the bearing capacity of the sediment equals the buoyant weight of the cylinder (Simpson et al., 1974). The ultimate bearing capacity, q_{ult} is given by Terzaghi et al. (1996)

$$q_{ult} = N_c c + \gamma^{'} e_o N_q + 0.5 N_\gamma w \gamma^{'} \tag{1}$$

where e_o is the initial embedment of the cylinder into the sediment, w is the width of the cylinder in contact with the sediment, and c is the cohesion. The buoyant unit weight of the sediment, $\gamma^{'}$is represented by

$$\gamma^{'} = \gamma_{sat} - \gamma_w \tag{2}$$

where γ_{sat} is the saturated unit weight of the sediment and γ_w is the unit weight of water. The variables N_c, N_q, and N_γ are bearing capacity factors that are dependent on the friction angle (ϕ) of the soil (Terzaghi et al., 1996). The relationship between these bearing capacity factors N_c, N_q, and N_γ and friction angle (ϕ) are written in the Supplementary material 1.

For fine-grained sediments, the friction angle is assumed to be zero, and all sediment strength is derived from cohesion. Fine-grained sediments do not dissipate excess porewater pressure on relevant time scales, meaning the soil behaves undrained during the initial placement. Hence, cohesion (c) or undrained shear strength (s_u) of the fine-grained particles can be used interchangeably. For $\phi = 0$, the bearing capacity factors are N_q= 1 and N_c= 5.7 from equations (S1) and (S2) in the Supplementary material 1. Thus, the bearing capacity equation reduces to

$$q_{ult} = 5.70 s_u + \gamma^{'} e_o \ . \tag{3}$$

For coarse-grained sediments, it is assumed that there is no cohesion. Therefore, the bearing capacity equation reduces to

$$q_{ult} = \gamma^{'} e_o N_q + 0.5 N_\gamma w \gamma^{'} \ . \tag{4}$$

The equation for bearing capacity was originally derived for rectangular objects; therefore, a modification was necessary to account for the semicircular contact surface provided by a cylinder laid on its side. It was assumed that the width of the contact surface could be approximated as the horizontal distance of the semicircular surface at the seabed. This width is described by the following relationship.

$$w = \begin{cases} 2\sqrt{2re_o - e_o^2} \ for \ e_o < r \\ d \ for \ e_o \geq r \end{cases} \tag{5}$$

where d is the diameter of the cylinder and r is the radius. Note, it is assumed that once the cylinder is embedded beyond the radius, the width in contact with the sediment will be equal to the diameter. Similar modifications have been made to the bearing capacity equation to compute the bearing capacity of sediment beneath the pipelines (Gao et al., 2013). The applied pressure acting on the seabed from the buoyant weight of the cylinder is then represented by

$$q_{app} = W_s^{'}/(wL) \tag{6}$$

where $W_s^{'}$is the buoyant weight and L is the length of cylinder. The buoyant weight of the cylinder is given by

$$W_s^{'} = W_s - B_w \tag{7}$$

$$W_s = M_s g \tag{8}$$

$$B_w = V\gamma_w = \rho_w g \pi r^2 L \tag{9}$$

where W_s is the weight and M_s is the mass of the cylinder in air, g is the acceleration due to gravity, B_w is the force of buoyancy due to water, V is the volume of the cylinder, γ_w is the unit weight of water, ρ_w is the water density, and r is the radius of the cylinder. The embedment of the cylinder, e_o can then be solved for by setting q_{ult} equal to q_{app}.

Objects placed on fine-grained sediments are expected to sink beyond the initial penetration due to consolidation settlement, i.e., dissipation of pore water pressure and drainage of water (Simpson et al., 1974). The amount of consolidation settlement, e_{ct}, undergone in time, t,

after initial embedment, e_o, is expressed in terms of the primary ultimate consolidation settlement, $e_{c\infty}$, and average degree of consolidation, U as

$$e_{ct} = e_{c\infty}\frac{U\%}{100} . \tag{10}$$

The total embedment, e_t, after time t can then be computed by the following relation as

$$e_t = e_o + e_{ct} . \tag{11}$$

The detailed expressions regarding the computation of consolidation settlement are presented in the Supplementary material 1.

2.1.2. Freefall deployment

A cylindrical object could fall as vertical, spiral, flip, horizontal, and seesaw (Abelev and Valent, 2004). Highest velocities and deepest embedments due to impacts occur when the cylinder falls vertically (Taber, 1999). Therefore, only the two extreme cases of vertical and horizontal fall and impact are considered. The cylinder is assumed to be released from just below the water surface in a predetermined orientation of either vertical or horizontal and to remain in the same orientation during the fall. The force equilibrium equation describing the motion of the cylinder in water is

$$M_s\frac{d^2z_w}{dt^2} = W_s - B_w - D_w \tag{12}$$

where z_w is the distance traveled in the water column and t is the time of fall. M_s, W_s, B_w and D_w are the mass, weight of the cylinder, buoyancy and drag force due to water respectively with

$$D_w = 0.5C_{dw_{tip}}\rho_w v^2 A_{tip} \tag{13}$$

where $C_{dw_{tip}}$ is the drag coefficient due to water on the projected face, ρ_w is the density of water, v is the velocity of fall in the water column, and A_{tip} is the projected area perpendicular to the direction of fall.

Eq. (12) is integrated to compute the impact velocity of the cylinder on the seabed surface. The depth traveled by the cylinder into the soil when the object finally comes to rest is the depth of penetration or embedment. The force equilibrium equation describing the travel of the object in sediment as presented in Chow et al. (2017) is

$$M_s\frac{d^2e_0}{dt^2} = W_s - B_w - B_s - F_{tip} - F_{shaft} - D_s \tag{14}$$

where B_s is the buoyancy due to effective weight of the displaced soil, F_{tip} is the tip resistance at the circular tip of the object, F_{shaft} is the shaft resistance from the shaft surface area of the object in contact with the soil, D_s is the drag resistance against the motion into the seabed soil. e_0 is the embedment depth and t is time. These terms are discussed in detail in the Supplementary material 1. Eq. (14) is integrated once to obtain the velocity of cylinder and integrated twice to compute the displacement inside the sediment. This displacement is therefore the embedment depth, which when normalized by the diameter or length depending on the freefall type yields the percent embedment (PE) which will be used frequently in this paper. For the study, it was assumed that the object being deployed was a 60 kg cylinder with a 20 cm diameter, 60 cm length, and the water depth was 10 m. These numbers are somewhat arbitrary and can be replaced by other values if desired.

2.2. Probabilistic approach

A probabilistic approach was used to quantify the embedment so that the soil properties can be represented by random variables (RVs). Specifically, a Monte Carlo simulation was applied to analyze the effects of sediment characterization and different soil strengths.

The first RV is the saturated unit weight γ_{sat} of the soil. It was assumed to follow a normal distribution (Sivakumar Babu and Srivastava, 2007; Forrest and Orr, 2010). For simulation purposes, the normal distribution was truncated to prevent the generation of unrealistic values. The minimum bound was set to γ_{sat} =12 to and the maximum bound was set to 22 kN/m^3. An example of the probability density function for γ_{sat} can be found in Fig. 2. The saturated unit weight is related to the buoyant unit weight, γ', as defined by Eq. (2). Hence, the randomly generated values of saturated unit weight are then converted into buoyant unit weight. The buoyant unit weight is then used in the bearing capacity equation (i.e. Eq. (1)) or the components of the force equilibrium equation (i.e. Eq. (14)) to compute the embedment and percent embedment (PE).

For cohesive soils, the second RV that needs to be addressed is cohesion (c). Note that for undrained analyses, it is assumed that the friction angle is zero, and that the cohesion is equal to the undrained shear strength (s_u) of the soil. It is well known that the s_u of offshore clays typically increases with depth as the vertical effective stress increases (Mackillop et al., 2016; Yang et al., 2019). The relation known as the undrained strength ratio (USR) is often used to characterize the shear strength of soils as a function of depth (Mackillop et al., 2016; Tan, 2004; Yang et al., 2019),

$$USR = s_u/\sigma'_{v0} = (USR)_{NC}{}^*(OCR)^m \tag{15}$$

where

$$\sigma'_{v0} = \gamma' z \tag{16}$$

and $(USR)_{NC}$ is the USR at an OCR of 1. OCR is the over consolidation ratio, m is the experimentally determined soil specific material coefficient, which is related to the rate of strength increase, σ'_{v0} is the vertical effective stress, and z is the depth of the soil. These parameters are typically obtained from laboratory testing using the SHANSEP procedure (Ladd and Foott, 1974).

A detailed literature review was conducted to collect typical values for the $(USR)_{NC}$ and m parameters in the SHANSEP equation from offshore environments around the world. In total, 29 sets of the two SHANSEP parameters were compiled (See Supplementary material 2, Table S1 for data of $(USR)_{NC}$ and m, and the sources) and used to develop a bivariate normal distribution. A bivariate distribution was desired because both $(USR)_{NC}$ and m parameters are soil specific parameters, meaning that they are likely correlated. Using a bivariate normal distribution for the Monte Carlo simulation ensures that the randomly generated two-parameter samples will be correlated as appropriate. Fig. 2 shows the randomly generated samples, and selected data pairs obtained from the literature review.

Note that using this approach assumes s_u= 0 kPa at the seabed surface. This is a common assumption in many geotechnical applications, however since the embedment process is localized to the upper portion of the sediment, assuming the shear strength at the seabed is zero would likely result in overpredictions of embedment. Therefore, data on the initial shear strength (s_{u0}) was compiled from offshore s_u profiles around the world (See Supplementary material 2, Table S3 for data of s_{u0}, and the sources) and a normal distribution was developed from that data. A total of 37 data points were used to develop the distribution which is shown in Fig. 2. Note, the distribution is truncated with a minimum bound of 0 and no upper bound. Therefore, similar to the relation proposed by Li et al. (2015), s_u with depth is then calculated by:

$$s_u = (USR)\sigma'_{v0} + s_{u0} . \tag{17}$$

Using this approach, the Monte Carlo simulation can randomly generate s_u profiles to be used in the embedment calculations. Fig. 3 shows an example of the generated profiles overlayed with selected generalized s_u profiles from different offshore sites.

For cohesionless soils, the effective stress friction angle ϕ' is modeled as a RV that follows a normal distribution (Sivakumar Babu and Srivastava, 2007; Forrest and Orr, 2010). A positive correlation between

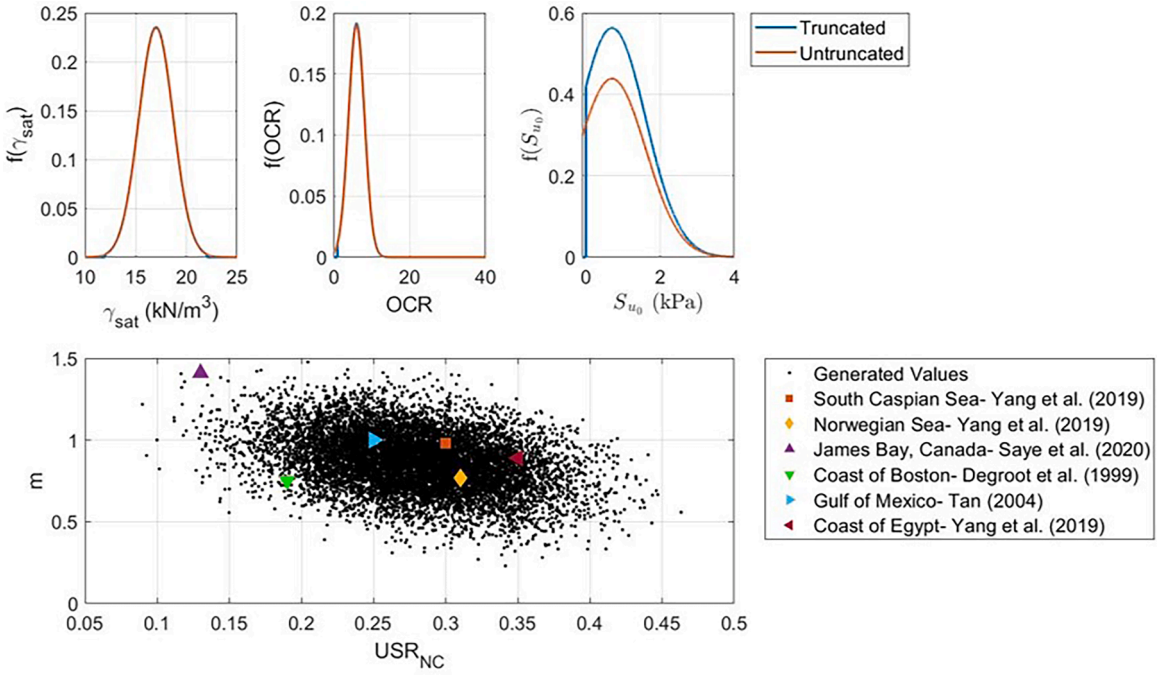

Fig. 2. Example of the input probability distributions of γ_{sat} (top left), **OCR** (top center) (See Supplementary material 2, Table S2 for data of **OCR** and the sources), $\mathbf{s_{u0}}$ (top right) (See Supplementary material 2, Table S3 for data of $\mathbf{s_{u0}}$, and the sources), and a scatter plot of the generated values of $(\mathbf{USR})_{NC}$ and **m** (See Supplementary material 2, Table S1 for data of $(\mathbf{USR})_{NC}$ and **m**, and the sources) from the bivariate normal distribution (bottom) for the SHANSEP parameters. $(\mathbf{USR})_{NC}$ and **m** are experimentally determined soil specific material coefficients, which are related to the rate of strength increase. 10,000 SHANSEP parameters were generated for each trial from the probability distribution parameters obtained from data present in the Supplementary material 2.

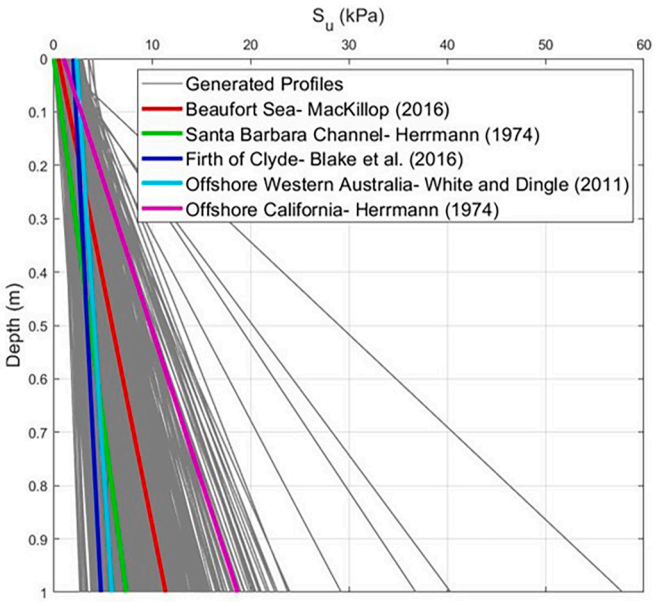

Fig. 3. Randomly generated undrained strength profiles overlaid by simplified profiles of undrained strength taken from offshore sites around the world (See Supplementary material 2, Table S1 for data of $(\mathbf{USR})_{NC}$ and **m**, and the sources; See Supplementary material 2, Table S2 for data of **OCR** and the sources; See Supplementary material 2, Table S3 for data of $\mathbf{s_{u0}}$, and the sources). 10,000 profiles were generated for each trial from the probability distribution parameters obtained from data present in the Supplementary material 2.

unit weight and friction angle is often assumed in the literature (Chowdhury and Xu 1993; Low and Tang, 1997a; Sivakumar Babu and Srivastava, 2007; Javankhoshdel and Bathurst, 2014). It is seen that soils with higher friction angles tend to possess higher saturated unit weights. The Pearson's correlation coefficient between the saturated unit weight and the friction angle was assumed to be 0.5 (Low and Tang, 1997a). Using this correlation coefficient, a bivariate normal distribution was constructed to generate random pairs of saturated unit weight and friction angle to be used in the embedment calculations. Note, the bivariate normal distribution was truncated at the previously defined bounds of saturated unit weight and at 28 and 50° for the friction angle. Fig. 4 shows an example of the randomly generated pairs of saturated unit weight and friction angle from the bivariate normal distribution.

2.3. Sediment characterization considerations

Three different tiers of seabed sediment characterization were investigated: 1) No Sediment Characterization 2) Sediment Type

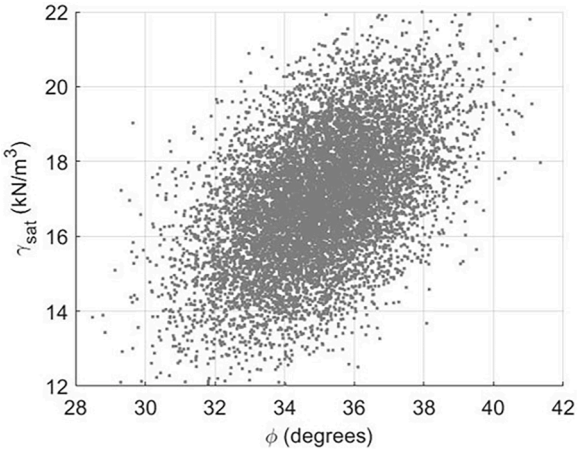

Fig. 4. Randomly generated 10,000 values of friction angle and saturated unit weight from the bivariate normal distribution. These values were generated every time for each trial.

Known, and 3) Geotechnical Testing Performed. The first tier of "No Sediment Characterization" means that the sediment conditions are unknown, and the sediment could be cohesive fine-grained or cohesionless sand. Bedrock, gravel, or vegetated seabed surfaces are excluded from this study. Sediment was then randomly chosen to be either cohesive or cohesionless in the simulations. Depending on whether the soil chosen is cohesive or cohesionless, a set of respective soil strength parameters were generated using coefficients of variation (*CV*) given in Table 1 and mean values. The coefficient of variation is a relative measure of variability and is expressed as a percentage. It is calculated by dividing the standard deviation by the mean and multiplying by 100. *CV* permits the comparison of variates free from scale effects (Brown, 1998). *CV* is used here to compare variability in percent embedment resulting from different sediment characterization techniques, deployment methods, and sediment strengths. The means of the sediment strength parameters were kept constant for all the three seabed sediment characterization levels and were as follows: 17 kN/m^3 for saturated unit weight (γ_{sat}), 6 for *OCR*, 0.7 kPa for initial undrained shear strength (s_{u0}), and 35° for friction angle (ϕ') and applied as described in the previous sections to predict values of embedments and percent embedments (*PE*). A total of 10,000 simulations were run and a distribution of *PE* was derived. The second tier of characterization "Sediment Type Known" signifies that the sediment is known to be cohesive or cohesionless. Such information could be derived from geoacoustic surveying, sampling, or geological records. *CV*s of random variables shown in Table 1 were used for both the cohesive and cohesionless soils. The third tier of characterization "Geotechnical Testing Performed" assumes a detailed geotechnical investigation through in situ testing and/or laboratory testing, and thus, that the sediment strength parameters were determined to the accuracy of methodology. Therefore, the *CV*s of the sediment strength parameters were reduced to values common for geotechnically tested soils (Duncan, 2000). For each of the sediment characterizations, 10,000 simulations were completed, histograms of *PE* were developed and means and *CV*s of *PE* were computed and presented in Fig. 5.

2.4. Sensitivity study

The sensitivity of embedment predictions on the different sediment strength parameters was studied. Monte Carlo simulation was applied to investigate distributions of *PE* for sites with different soil strengths. This was tested in four different trials in which the mean embedment was computed for a soft clay, stiff clay, loose sand, and a dense sand (Table 2). To model these conditions, the mean values of the sediment strength parameters were varied while the *CV*s were held constant. For simplicity, it was assumed that the *CV*s of the strength parameters would be equal to the *CV*s for the "Geotechnical Testing Performed" case shown in Table 1. The mean values of the strength parameters used in the sites with different soil strengths can be found in Table 2.

2.5. Consolidation

Time dependent embedment predictions were studied by incorporating the consolidation settlement. For fine-grained soils, the Monte Carlo simulation was applied to investigate distributions of *PE* for different time durations of interest. The study was performed for the case of object deployment by careful placement and under the sediment characterization "Sediment Type Known: Cohesive". It was assumed the consolidation settlement contributions are insignificant for freefall installations. The time durations of interest were $t = 0$, 30 days (1 month), 365 days (1 year), and 730 days (2 years) taken as standard times. To model a single condition of a certain time duration, first the ultimate primary consolidation settlement was computed using the equation (S4) in the Supplementary material 1. Then the consolidation settlements at different time durations of interest were computed using Eq. (10) and equations (S4) – (S9) in the Supplementary material 1. The total embedment was calculated using Eq. (11) and finally the Percent Embedment was calculated by dividing by the diameter and multiplying by 100.

Table 2
Summary of mean values of sediment strength parameters for each trial.

Soil Strength	μ of γ_{sat} (kN/m^3)	μ of *OCR*	μ of s_{u0} (kPa)	μ of ϕ' (°)
Soft Cohesive	14	1.1	0.1	–
Stiff Cohesive	18	8	1.2	–
Loose Cohesionless	16	–	–	32
Dense Cohesionless	21	–	–	40

3. Results and discussion

Results of embedment predictions for the model cylinder were performed and quantified as percent embedment. They are shown and described in the following three sub-sections. The first sub-section is related to the results of embedments at varying levels of prior knowledge of seabed sediment conditions. The second sub-section pertains to the embedment predictions for the cases of different sediment strength. The third sub-section is related to the time dependent embedment predictions of model cylinders deployed in cohesive sediments. Finally, results are discussed in the context of validation bv comparison to free fall penetrometer and cylindrical anchor deployments available from the literature and also from single case studies.

3.1. Sediment characterization considerations

Fig. 5 shows the stairstep histograms (outline of the histograms) of percent embedment predicted for the three seabed sediment characterizations (indicated by the different colors used) for the carefully placed deployment (Fig. 5 top), the vertical impact (Fig. 5 center), and the horizontal impact (Fig. 5 bottom). Left panels in Fig. 5 depict cohesive soils and right panels show cohesionless soils. The distributions for unknown sediment information (Fig. 5 blue) are the same for panels in the respective rows of Fig. 5. Fig. 6 depicts the trend of the statistical parameters like mean, standard deviation and *CV* for the sediment characterization scenarios and deployment methods in the same order as that of Fig. 5.

Figs. 5a and 6a illustrate the results for the case that the cylinder is placed carefully on cohesive soils. For the case of *No Sediment Characterization (NSC)*, the mean of *PE* (μ_{PE}) is 7.2 %, the standard deviation of *PE* (σ_{PE}) is 8.3 %, and the coefficient of variation (CV_{PE}) is 115.2 %. If the sediment type is known (here: *Sediment Type Known (STK)-Cohesive*), μ_{PE} is 11.1 %, σ_{PE} is 10.8 %, and CV_{PE} is 97.3 %. For *Geotechnical Testing (GT)-Cohesive*, μ_{PE} is 11.5 %, σ_{PE} is 3 %, and CV_{PE} is 26.1 %. μ_{PE} is smallest for the case of *NSC*. A low mean of *PE* could represent a problem in terms of underprediction of embedment for applications such as sensor performance. The uncertainty is indicated as high through the

Table 1
Summary of coefficient of variation values of sediment strength parameters for each trial.

Sediment Characterization	CV of γ_{sat} (%)	CV of *OCR*(%)	CV of s_{u0} (%)	CV of ϕ' (%)
No Sediment Characterization	10	35	130	5
Sediment Type Known	10	35	130	5
Geotechnical Testing Performed	3	10	20	2

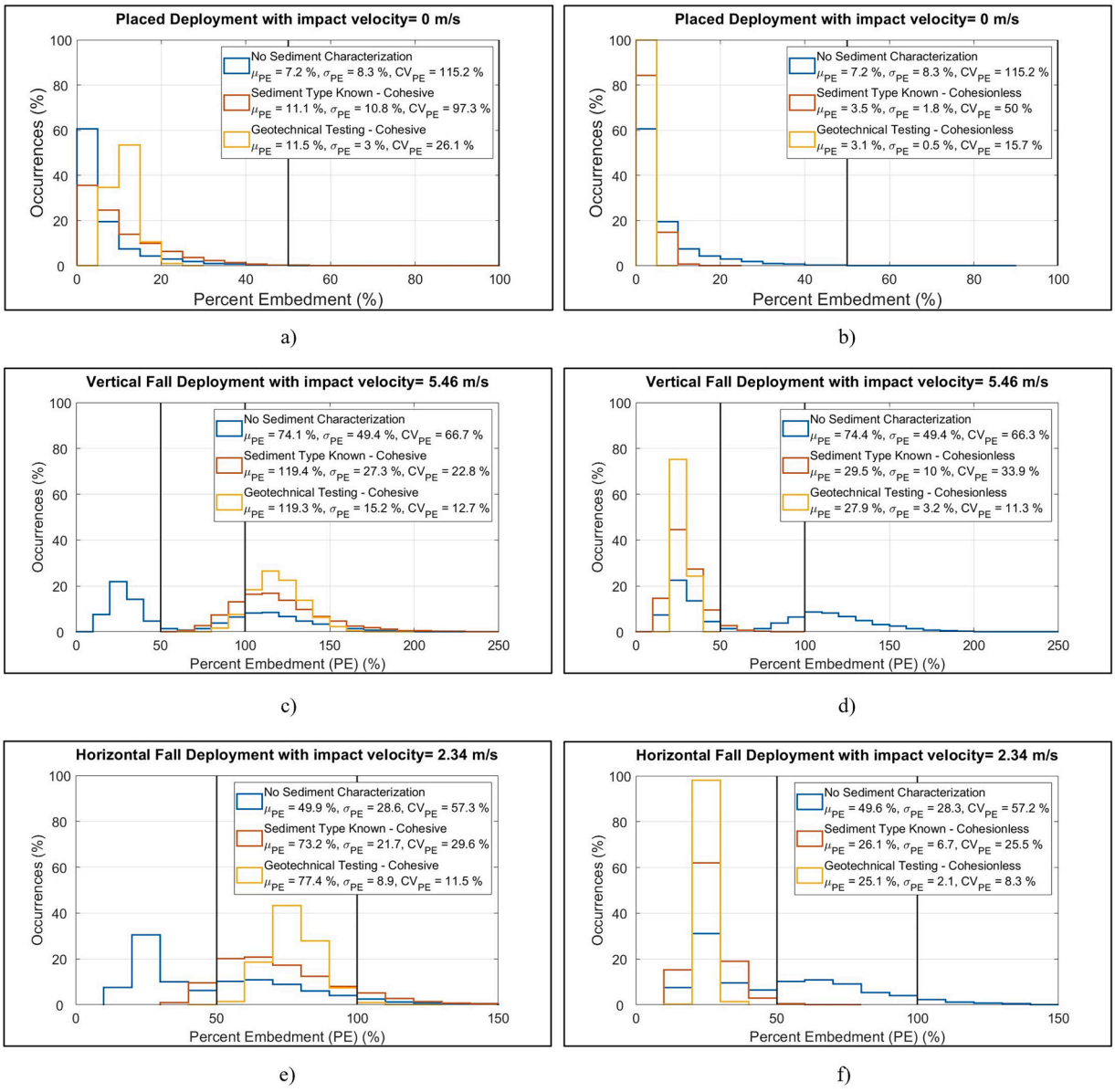

Fig. 5. Stairstep histogram of percent embedment under cases of No Sediment Characterization, Sediment Type Known and Geotechnical Testing Performed when sediment is - (a) cohesive (placed deployment) (b) cohesionless (placed deployment) (c) cohesive (vertical fall) (d) cohesionless (vertical fall), (e) cohesive (horizontal fall), and (f) cohesionless (horizontal fall).

CV_{PE}, as would be expected for the case of *NSC*. Thus, likelihood of underprediction and high uncertainty highlight the significant risks associated with a complete lack of seabed information. Between the cases of *STK* and *GT*, the derived mean is approximately similar, but the σ_{PE} and the CV_{PE} decrease significantly for *GT*. Importantly, looking at Fig. 6a, it is clear that an underprediction of *PE* may still occur for a noticeable number of simulations. For the case of careful object placement on cohesionless sediment (Fig. 5b), all site investigation tiers suggest $>$ 50 % chance of little ($<$ 10 %) embedment with *STK* even placing $>$ 80 % of simulations in this category. Going with the somewhat arbitrary assumption that a carefully placed sensor would have a full performance failure at 100 % embedment and a significant performance loss at 50 % embedment, the data suggest that through careful placement (impact velocity $=$ 0 m/s), any site investigation may become unnecessary since the chance of embedment $\geq$ 50 % during placement are generally unlikely. Fig. 6b indicates that both the mean and standard deviation of *PE* decrease, however, the decrease in standard deviation from *NSC* to *STK* is greater than that of *STK* to *GT*. Consequently, the decrease in variability is seen higher when geophysical investigations are done, but only further decreased to a lesser extent by geotechnical testing.

Figures (e) and (f) of both Figs. 5 and Fig. 6 depict the horizontal impact with a similar impact surface as previously discussed but an impact velocity of 2.34 m/s. A change in scale should be noted. The higher impact velocity leads to deeper penetration depths moving the simulations beyond the arbitrary performance thresholds at 50 % and 100 % embedment. *NSC* yielded $\mu_{PE} \approx$ 50 %, representing an overprediction if cohesionless sediments would be true and an underprediction if cohesive sediments would be true. *STK* and *GT* both suggest $\mu_{PE} \approx$ 75 % for cohesive sediments and $\mu_{PE} \approx$ 25 % for cohesionless soils with little likelihood for embedment exceeding 50 % for cohesionless soils and little likelihood for embedment being smaller than 50 % or exceeding 100 % for cohesive soils. This means that for the sensor performance problem focused on herein, *GT* would have few benefits. However, the reader is reminded if embedment needs to be predicted more accurately, the standard deviations associated with a specific test

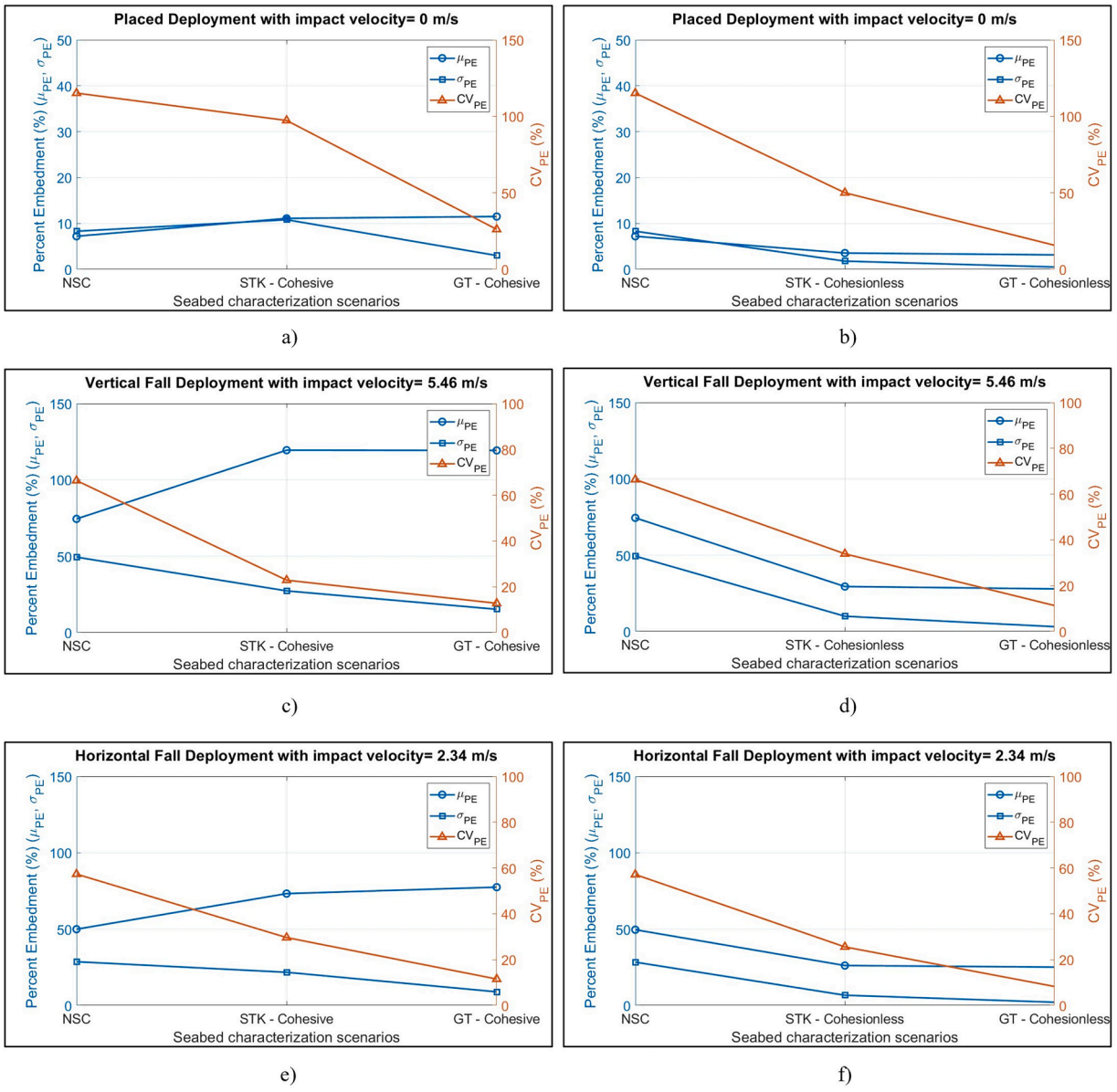

Fig. 6. Trend of statistical parameters of percent embedment under cases of No Sediment Characterization, Sediment Type Known and Geotechnical Testing Performed when sediment is - (a) cohesive (placed deployment) (b) cohesionless (placed deployment) (c) cohesive (vertical fall) (d) cohesionless (vertical fall), (e) cohesive (horizontal fall), and (f) cohesionless (horizontal fall).

are significantly smaller than the distributions depicted in Fig. 5. In Fig. 6e, both *STK* and *GT* have similar means, however, the CV_{PE} reduces significantly by about 20 %. While comparing the statistics for a horizontal impact into cohesionless sediments (Fig. 6f) to that for a horizontal impact into cohesive sediments (Fig. 6e), even though the trend of μ_{PE} with improved sediment characterization in Fig. 6f is opposite to that of Fig. 6e, the drop in σ_{PE} with improved sediment characterization is higher in Fig. 6f. As a result, the nature of CV_{PE} is similar in both the figures. Hence, it shows that geotechnical testing yields the most accurate prediction of embedment, as expected.

Finally, (c) and (d) of both Figs. 5 and 6 illustrate the vertical impact with an impact velocity of 5.46 m/s. The impact velocity is highest for this method of deployment which leads to even deeper penetration depths displacing the histogram results more towards the right of the x-axis. *NSC* yielded $\mu_{PE} \approx 75$ %, expressing an overprediction if cohesionless sediments would be true and an underprediction if cohesive sediments would be true. *STK* and *GT* both suggest $\mu_{PE} \approx 120$ % for cohesive sediments and $\mu_{PE} \approx 28$ % for cohesionless soils with still minimum likelihood (similar as in Fig. 5f) for embedment exceeding 50 % for cohesionless soils and maximum likelihood for embedment exceeding 100 % for cohesive soils. This makes prediction with *NSC* truly a flip-of-a-coin regarding sensor performance, while *STK* and *GT* make reliable predictions for cohesionless soils. Generally, the results suggest that when sediment type is known, the variability reduces by about 45 % over no sediment information. And performing geotechnical testing reduces the variability in prediction of *PE* by an additional 10 % over just the sediment type identification. On examining Fig. 6c and d), it can be noted that there is a heavy reduction in μ_{PE} under *STK* for cohesionless soil compared to cohesive soil, which is due to the high bearing capacities of cohesionless soil (Terzaghi et al., 1996). As a result, the μ_{PE} for *STK* and *GT* in d) are always below 50 % for cohesionless soils. This high bearing capacity combined with the small variability of sediment strengths for cohesionless soils as seen in Table 1 results in smaller σ_{PE} and therefore significant decrease (20 %) in CV_{PE} when going from *STK* to *GT*. Since the *PE* occurrences are almost always smaller than 50 % in cohesionless soils, the added service of reduced

variability by *GT* does not provide much advantage to the sensor performance problem discussed herein. However, Fig. 6c shows that the higher chances of *PE* in cohesive soils exceeding the sensor dimensions is indicated by *STK*. This means *STK* may be sufficient to predict a high possibility of diminished sensor performance, and if the site investigation is focused on the sensor performance problem solely, *GT* would have few benefits. However, if a more specific prediction of penetration depth were needed, *GT* would provide the best prediction.

3.2. Sensitivity study

Four different trials were run for soft clay, stiff clay, loose sand, and dense sand (see Table 2 and third row of Table 1). Fig. 7a to f represent the histograms of the *PE* when the sediment is characterized in terms of consistency as soft or stiff cohesive soil (e.g., high water content and low bulk density) or in terms of packing as loose or dense cohesionless sand. Fig. 7a and b represent results for cohesive and cohesionless sediments respectively under placed deployment. Similarly, Fig. 7c and d represent results for cohesive and cohesionless sediments respectively under vertical fall deployment and 6 e) and f) represent results for horizontal fall deployment. On comparing Fig. 7, μ_{PE} reveals that the packing state of the soil has a significant impact on all cases with μ_{PE} increasing by at least three times and up to about 25-times from dense to loose soils. Regarding cohesionless soils, embedments are predominantly less than 50 % with only some risk of embedment larger than 50 % for loose sands and the highest speeds/ lowest penetration surface area investigated. However, impacts of seabed consistency in cohesive soils are significant. For carefully placed sensors, sediment stiffness may decide if the sensor is embedded < 20 % or > 100 %. For horizontally falling cylinders, embedment may change from ~ 50 % to > 200 %, while for the vertically falling cylinders, embedment > 100 % is likely and embedment may reach ~ 300 %.

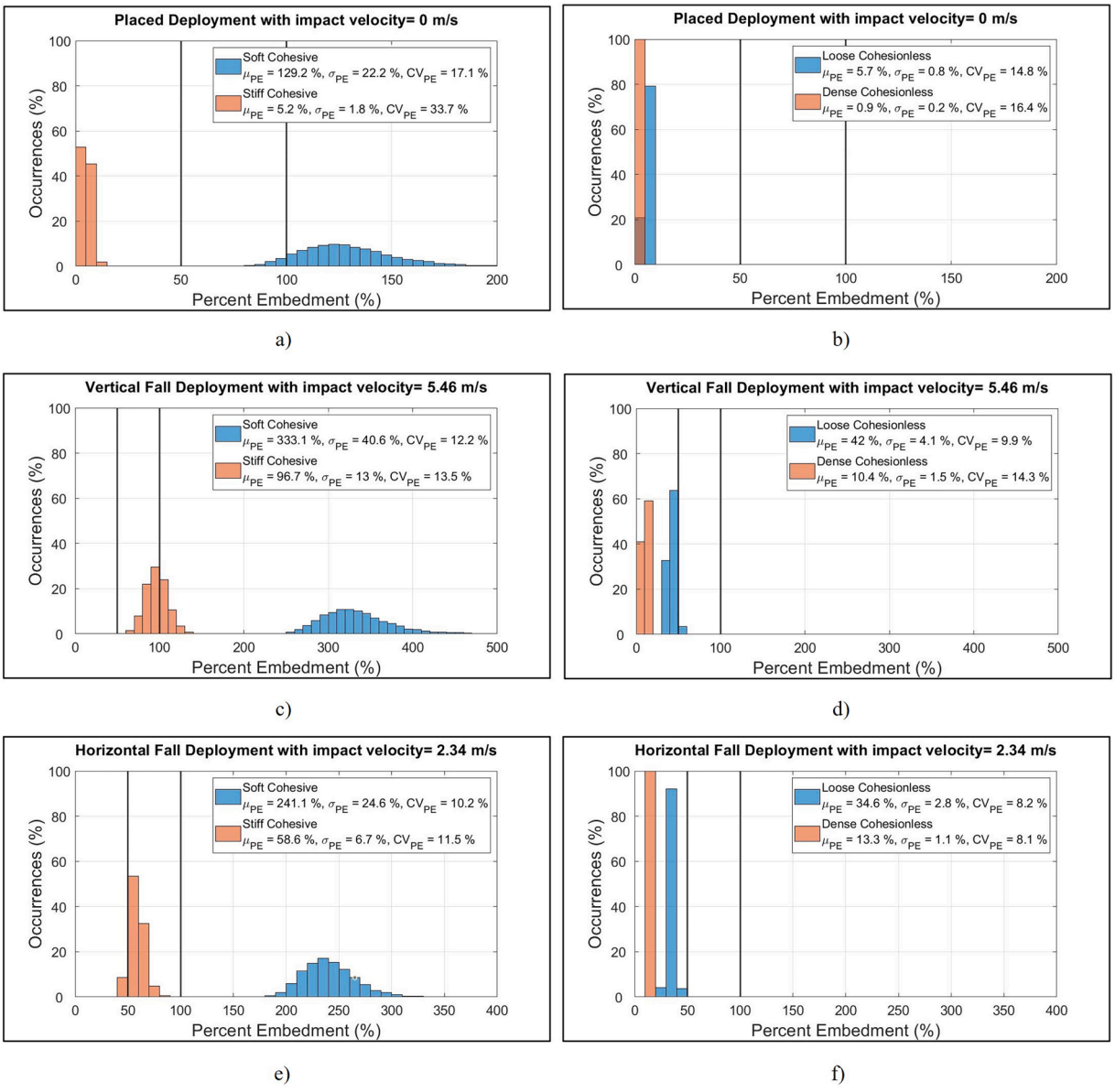

Fig. 7. Histogram of percent embedment under cases of different sediment strengths as either soft or stiff cohesive and loose or dense cohesionless when sediment is- (a) cohesive (placed deployment) (b) cohesionless (placed deployment) (c) cohesive (vertical fall) (d) cohesionless (vertical fall), (e) cohesive (horizontal fall), and (f) cohesionless (horizontal fall).

3.3. Consolidation

Consolidation is a common phenomenon seen in cohesive sediments. The magnitude of consolidation settlement of cylinders is small compared to the initial embedment by freefall. Hence, consolidation settlements were only calculated and shown for the case of placed deployments. Fig. 8 shows the results of total percent embedment (sum of initial *PE* and *PE* due to consolidation settlement) after a certain time t for cohesive sediments. Fig. 8a shows the histogram of total *PE* after time $t = 0$ days, which means it is equivalent to the initial *PE*. A change in the shape of the histogram can be observed after $t = 30$ days (Fig. 8b) with μ_{PE} changing from 11.1 % to 14.5 %, which is a percentage increase of 31 % from the initial value. σ_{PE} changes from 10.6 % to 9.2 %, CV_{PE} changes from 95.8 % to 63.6 %. Thus, the variability of *PE* is reduced since a low embedment is less likely. The change in *PE* however slows down for $t =$ 365 days (Fig. 8c) as μ_{PE} changes from 14.5 % to 16.5 %, which is an additional percentage increase of 18 % over a period of 11 months. This change of 18 % over a period of 11 months is smaller compared to a change of 31 % over the initial month. No significant changes occur after a period of 1 year (Fig. 8d), being in line with expectations for a light object such as the cylinder investigated here.

3.4. Validation of results

Few studies have measured the *PE* of cylinders into the seabed from impact or placements. Furthermore, the methods used to calculate *PE* represent standard methods and theories commonly applied for a wide range of offshore engineering applications. Therefore, no specific field or lab testing was performed to test the validity of the embedment prediction equations and models used, but validation was performed to test the stochastic analysis in two ways: 1) by comparison to free fall penetrometer and cylindrical anchor deployments available from the literature, and 2) by single case prediction using seabed soil information from the literature.

Fig. 9a shows the distributions of *PE* for portable free-fall penetrometer (PFFP) deployments on a mud flat in the Great Bay estuary by Paprocki et al. (2024). The PFFP measures 0.63 m in length, 0.0875 m in diameter, and weighs 7.71 kg. It was deployed with a conical tip which is expected to yield a deeper penetration than a blunt cylinder. The drop height was 4 m. The average soil properties determined in the study were γ_{sat} of 12.8 kN/m^3, s_{u0} of 0.7 kPa, s_u/z of 3.5 kPa/m. s_u/z was used in Eqs. (15) and (16) to back-calculate *USR* equal to 1.27. Applying typical values of $(USR)_{NC}$ as 0.24 and m as 0.8 in Eq. (15), *OCR* was calculated as 8.025. These values were treated as the mean values of sediment strengths while the *CVs* corresponding to *GT* were taken from Table 1. The prediction of *PE* for the particular PFFP under *GT* in these soil conditions was plotted as a histogram and the *PE* related to actual measurements were plotted as scatter plots of red marks well inside the histogram. Fig. 9a clearly shows that there is good agreement between the predictions and the actual measurements.

O'Beirne et al. (2015) studied the capacity of dynamically installed anchors through field testing and three dimensional large-deformation finite element analysis. The anchor used has a diameter of 0.06 m, length of 0.75 m, and a mass of 20.69 kg. Different drop heights were used, however, the histograms prepared were for the 3 m drop height, which were the most abundant. The study established average soil properties, including a γ_{sat} of 10.8 kN/m3, s_{u0} of 0 kPa, s_u/z of 1.5 kPa/m for the upper 1.5 m layer and 0.8 kPa/m for the layer below. Following the same back calculation procedure as discussed earlier for the study of Paprocki et al. (2024), *OCR* was calculated as 14.51. Treating these values as the mean sediment strengths, while the coefficients of variation (*CVs*) corresponding to *GT* were extracted from Table 1. A histogram depicting the prediction of *PE* for the specific anchor under *GT* in these soil conditions was plotted, and scatter plots of red marks, well

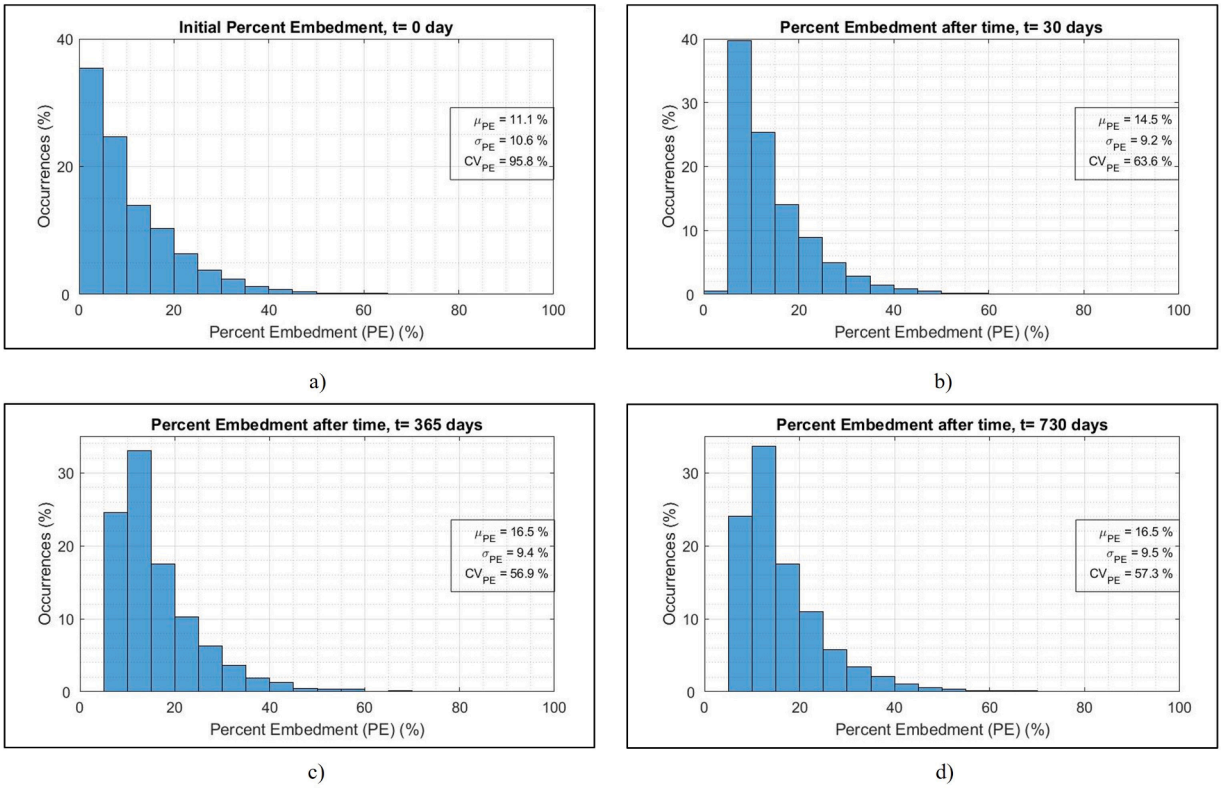

Fig. 8. Histogram of Total Percent Embedment at times, (a) $t = 0$ days, (b) $t = 30$ days, (c) $t = 365$ days, and (d) $t = 730$ days after placed deployment (i.e. impact velocity= 0 m/s) under the case of Sediment Type Known- Cohesive.

Fig. 9. Histogram of predictions of *PE* of free fall penetrometers and dynamically installed cylindrical anchors on cohesive soils along with the experimental measurements made at (a) Great Bay estuary, New Hampshire, (b) Lower Lough Erne, Northern Ireland, (c) results upscaled from centrifuge tests, and (d) Campos basin, Brazil. (a) is related to free-fall penetrometer deployments. (b), (c), and (d) are related to dynamically installed anchors.

within the histogram, illustrated the relationship between the predicted and actual measurements. Fig. 9b distinctly indicates a strong agreement between the predictions and the actual measurements.

Similarly, O'loughlin et al. (2009) performed centrifuge lab tests on a small dynamically installed anchor, whose results were upscaled to a prototype of diameter 1.2 m, length 15 m, and a mass of 118 tons. The drop height was 30 m. The soil was normally consolidated with a γ_{sat} of 16.56 kN/m^3, s_{u0} of 0 kPa, and s_u/z of 1.15 kPa/m. Following the similar procedure of back calculation and statistics of soil properties as done for previous studies, a histogram showing the prediction of *PE* was plotted, as shown in Fig. 9c and the actual *PE* upscaled from the lab tests were plotted as red scatter marks. The positioning of these actual *PE* within the predictions shows that there is a good agreement between the predictions and actual embedments. Medeiros (2002) as cited in Jeanjean et al. (2012) reported a field test in Campos basin, Brazil using a torpedo anchor weighing 40,777 kg, 12 m long and a 0.76 m diameter in a soil of s_{u0} of 5 kPa, and s_u/z of 2 kPa/m. The predicted *PE* histogram and measured *PE* as shown in Fig. 9d demonstrates a good match.

The results of predicted and measured *PE* were also carried out for cohesionless soil and is indicated through histograms and scatter plots in Fig. 10. The *PEs* were measured using a different PFFP at several sandy sites, specifically the windfarm Alpha Ventus (North Sea), Waimanalo Bay (Hawaii), and Kailua Bay (Hawaii) by Stark et al. (2009;2012). The PFFP measures 0.11 m in diameter, 0.81 m in length with a mass of 13 kg. It was equipped with a conical tip, anticipating a greater depth of penetration compared to a blunt cylinder. At Alpha Ventus, the water depth was ≈ 30 m, with sand of ϕ' 32°, γ_{sat} of 19.9 kPa. Applying the friction angle and saturated unit weight of the literature as means and using the CVs corresponding to *GT* listed in Table 1, the *PE* was predicted under the case of *GT* and shown in Fig. 10a. The freefall penetration depth measurements were in the range of 0.07- 0.11 m which corresponded to 8- 13 % of *PE*. The location of experimental measurements well within the histogram indicate a very good agreement of the prediction carried out.

Stark et al. (2009, 2012) performed PFFP deployments at Waimanalo Bay, Hawaii where the sediments were composed of medium to coarse sand of ϕ' equal to 34°, γ_{sat} of 18.7 kPa. Utilizing the literature's mean friction angle and saturated unit weight, along with the GT-associated coefficients of variation from Table 1, PE was predicted in the GT scenario (Fig. 10b). The measured freefall penetration depths ranged from 0.12 to 0.2 m, corresponding to 14 to 24 % of PE. The experimental measurements are slightly higher than the predictions which might possibly be a result of greater depth of penetration obtained due to conical tip compared to a blunt cylinder. And the availability of only 4 *PE* datapoints in Waimanalo Bay could have represented some biasness in measurements.

A similar study was done by Stark et al. (2009, 2012) in Kailua Bay, Hawaii. The sediments were comprised of very fine to medium sand with a ϕ' of 30° and a γ_{sat} of 22.2 kPa. Using the literature's mean friction angle and saturated unit weight, along with GT-associated coefficients of variation from Table 1, PE was predicted in the GT scenario (Fig. 10c). The experimental measurements falling well within the histogram signify a high level of agreement with the conducted predictions.

The *PE* measurements for both the cohesive and cohesionless sediments for corresponding PFFPs and anchors almost always fell within the predicted *PE* histograms obtained through sediment data from the corresponding literature, supporting the accuracy of this work.

Secondly, we assumed a case of cohesive sediments Yang et al. (2019) for $OCR = 1.2$ and $s_{u0} = 1$ kPa; Paniagua and L'Heureux (2019) for γ_{sat} = 19 kN/m^3) and a case of sandy seabed characterization (Brandes et al. (2002) for $\phi' = 37°$ and γ_{sat} = 18.64 kN/m^3) and we assumed a cylinder of the geometry and weight assumed in previous predictions in this study (refer to deployment methods section). Calculating the *PE* for those two cases based on the equations presented

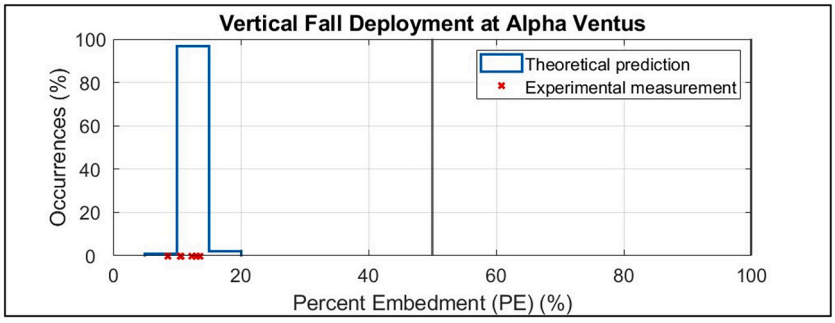

a)

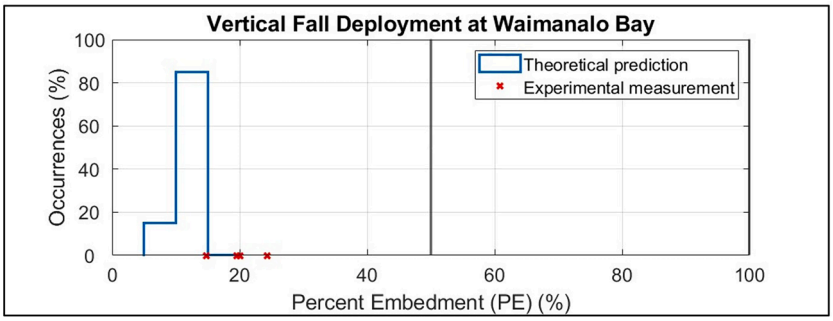

b)

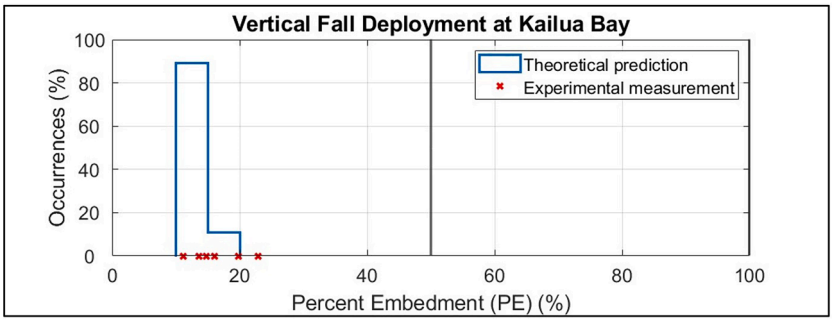

c)

Fig. 10. Histogram of predictions of *PE* of free fall penetrometers on cohesionless soils along with the experimental measurements made at (a) Alpha Ventus, North Sea, (b) Waimanalo Bay, Hawaii, and (c) Kailua Bay, Hawaii.

previously which represent accepted standard procedures in geotechnical engineering yield a *PE* of 82.7 % and 17.8 %, respectively, which fall well within our stochastic predictions (refer to *PE* histogram panels c) and d) respectively in Fig. 5).

4. Conclusion

The embedment of objects deployed on the seafloor can have significant performance impacts for the specific object, e.g., sensors or anchoring infrastructure. Here, the problem of a sensor to be placed on the seabed was arbitrarily assumed. The sensor would experience significant performance loss for embedment > 50 % of the sensor and total performance failure for embedment > 100 %. While a detailed geotechnical seabed sediment characterization is always desirable, this can be prohibited by costs, access, timing, and other reasons. This study utilized Monte Carlo simulation to assess the importance of seabed site investigation considered as three tiers: *No Sediment Characterization (NSC)* (i.e., it is cohesive mud or cohesionless sand at a 50–50 % chance), *Sediment Type Known (STK)* (i.e., it is known if sediments are cohesive or cohesionless from, e.g., geoacoustic surveying or geological sediment maps), and *Geotechnical Testing (GT)* has been performed. The model was then used to analyze the effects of different sediment characterization qualities and the effects of varying sediment strengths on the prediction of embedment of a cylinder of arbitrary dimensions and weight for a careful placement with no impact velocity, a horizontal freefall and impact at > 2 m/s, and a vertical freefall with impacts at > 5 m/s. From these trials, the following conclusions can be drawn:

- A complete lack of any sediment characterization prior to deployment results in the highest variability in the embedment results. The variability decreases by about 65 % when the sediment type is known and performing geotechnical testing further reduces it by at least 15 %, sometimes even by 35 %.
- Based on the arbitrary assumption that a sensor would completely fail when fully embedded and experience significant performance loss when embedded halfway, the data indicates that if sensors are placed carefully (with an impact velocity of 0 m/s), there may be no need for a site investigation because the likelihood of embedment exceeding 50 % is generally low.
- For sensors deployed by horizontal free fall, cohesive sediments have $\mu_{PE} \approx 75$ %, while cohesionless sediments have $\mu_{PE} \approx 25$ %. The likelihood of embedment exceeding 50 % is low for cohesionless sand. However, for fine-grained, cohesive sediments, it is unlikely that embedments are smaller than 50 % or reach 100 %. In

addressing the sensor performance issue, *GT* would provide limited advantages. However, the reader is reminded that, for accurate predictions, *GT* is needed.

- When sensors are deployed by vertical free fall, cohesive sediments are likely to promote full embedment (> 100 %), whereas embedment is expected to remain below 50 % for cohesionless sediments. This makes predicting sensor performance with *NSC* a 50–50 chance, while *STK* and *GT* provide reliable predictions for cohesionless sediments. However, *GT* becomes particularly important for cohesive sediments.
- When the embedment results related to different sediment strengths are compared, μ_{PE} demonstrates that the sediment's consistency and packing state has a considerable influence in all cases, with μ_{PE} increasing by a minimum of 3 times to up to approximately 25 times from dense to loose sediments.
- For cohesionless sediment, the deployment method does not affect the embedment much as all the cases lead to embedment predominantly < 50 %. However, embedment in cohesive sediment is significantly affected by the choice of deployment method as embedment might range from 50 % to 300 %.
- μ_{PE} of consolidation results shows that consolidation settlements are significant within the first month after deployment and then slow down.

The model and results presented herein provide a framework for predicting the embedment of cylindrical objects deployed offshore for different tiers of sediment characterization. While this study focused on one specific offshore engineering problem, namely the embedment of a cylindric object into the seabed from shear failure and consolidation after placement and during impact, the presented framework is directly transferable to other seabed engineering problems, and thus, presents a pathway to assess the value of different tiers of site investigation in the context of a specific engineering problem. This is important to optimize planning, design, and management of ocean engineering efforts including seabed interaction.

This study was based on some assumptions, and therefore, has some limitations that influence the generalization of its findings. First, the investigation was conducted under hydrostatic conditions, which may limit the applicability of the results to dynamic marine environments. Additionally, the study assumed a consistent cylinder trajectory without accounting for tumbling effects expecting to simulate the extreme conditions for embedment. While the two impact orientations considered represent two boundary conditions, they may not represent the most likely orientation of impact unless the cylinder is designed to fall in a certain orientation, like e.g., the free fall penetrometers used for validation. The seabed topography was assumed as horizontal and the sediment types were either basic clay or sand, which constrain the study's representativeness of diverse marine conditions. However, these two types were chosen as the boundary conditions of seabed types that raise concern for embedment. Furthermore, the absence of soil stratification neglects an important aspect of underwater terrains, suggesting the need for future research to explore the influence of these factors for a more comprehensive understanding of embedment predictions in marine environments. The study is also based on data sets from the literature and did not include specific validation experiments. In fact, the authors were unable to find studies that specifically tested this scenario. The reason for this may be that presented methods to predict bearing capacity failure and consolidation are standard practice in geotechnical engineering, and thus, are not expected to represent an uncertainty in prediction. Instead, the knowledge of local site information and data are typically the concern regarding such predictions, as is investigated in this study.

Declaration of generative AI and AI-assisted technologies in the writing process

During the preparation of the initial draft of this work, ChatGPT 3.5 was used to assist with initial phrasing of single sentences. Since this initial draft, the authors reviewed and edited the contentand take full responsibility for the content of the publication.

CRediT authorship contribution statement

Saurav Shrestha: Conceptualization, Methodology, Software, Writing – original draft, Data curation. **Nina Stark:** Conceptualization, Methodology, Writing – review & editing, Supervision, Funding acquisition, Project administration. **Brendan Green:** Conceptualization, Methodology, Software, Writing – original draft, Writing – review & editing, Data curation. **Dan Stilwell:** Writing – review & editing, Supervision, Funding acquisition, Project administration. **Mingyu Kim:** Writing – review & editing.

Declaration of competing interest

The authors declare that they have no known competing financial interests or personal relationships that could have appeared to influence the work reported in this paper.

Data availability

The data of soil parameters used to obtain the probability distribution parameters for the generation of 10,000 data for each trial are present in the Supplementary material 2.

Acknowledgments

This work was supported by the Office of Naval Research [Grant Nos: N00014- 20- 1- 2845]. Any opinions, findings, and conclusions or recommendations expressed in this material are solely those of the authors.

Supplementary materials

Supplementary material associated with this article can be found, in the online version, at doi:10.1016/j.apor.2024.103948.

References

Abelev, A., Valent, P., 2004. Impact burial of cylinders in soft marine sediments. In: Proceedings of the ASCE Conference, Civil Engineering in the Oceans 6, pp. 419–433. https://apps.dtic.mil/sti/citations/ADA444550.

Albatal, A., Stark, N., Castellanos, B., 2020. Estimating *in situ* relative density and friction angle of nearshore sand from portable free-fall penetrometer tests. Can. Geotech. J. 57, 17–31. https://doi.org/10.1139/cgj-2018-0267.

Aubeny, C.P., Shi, H., 2006. Interpretation of Impact Penetration Measurements in Soft Clays. J. Geotech. Geoenviron. Eng. 132, 770–777. https://doi.org/10.1061/(ASCE)1090-0241(2006)132:6(770).

Brandes, H.G., Silva, A.J., Walter, D.J., 2002. Geo-acoustic characterization of calcareous seabed in the Florida Keys. Mar. Geol. 182, 77–102. https://doi.org/10.1016/S0025-3227(01)00229-8.

Brown, C.E., 1998. Coefficient of Variation. Applied Multivariate Statistics in Geohydrology and Related Sciences. Springer Berlin Heidelberg, Berlin, Heidelberg, pp. 155–157. https://doi.org/10.1007/978-3-642-80328-4_13.

Catano-Lopera, Y.A., Demir, S.T., Garcia, M.H., 2007. Self-burial of short cylinders under oscillatory flows and combined waves plus currents. IEEE J. Oceanic Eng. 32, 191–203. https://doi.org/10.1109/JOE.2007.890968.

Chen, J., Vissinga, M., Shen, Y., Hu, S., Beal, E., Newlin, J., 2021. Machine learning–based digital integration of geotechnical and ultrahigh–frequency geophysical data for offshore site characterizations. J. Geotech. Geoenviron. Eng. 147, 04021160 https://doi.org/10.1061/(ASCE)GT.1943-5606.0002702.

Chow, S.H., O'Loughlin, C.D., White, D.J., Randolph, M.F., 2017. An Extended Interpretation of the Free-Fall Piezocone Test in Clay. Géotechnique, pp. 1–14. https://doi.org/10.1680/jgeot.16.P.220.
Chowdhury, R.N., Xu, D.W., 1993. Rational polynomial technique in lope-reliability analysis. J. Geotech. Engrg. 119, 1910–1928. https://doi.org/10.1061/(ASCE)0733-9410(1993)119:12(1910).
Duncan, J.M., 2000. Factors of safety and reliability in geotechnical engineering. J. Geotech. Geoenviron. Eng. 126, 307–316. https://doi.org/10.1061/(ASCE)1090-0241(2000)126:4(307).
Forrest, W.S., Orr, T.L.L., 2010. Reliability of Shallow Foundations Designed to Eurocode 7, 4. Georisk: Assessment and Management of Risk for Engineered Systems and Geohazards, pp. 186–207. https://doi.org/10.1080/17499511003646484.
Friedrichs, C., Rennie, S., Brandt, A., 2016. Self-burial of objects on sandy beds by scour: a synthesis of observations. In: Proceedings of the Scour and Erosion. Presented at the The 8th International Conference on Scour and Erosion. Oxford, Uk. CRC Press, pp. 179–189. https://doi.org/10.1201/9781315375045-23.
Friedrichs, C.T., Rennie, S.E., Brandt, Al., 2018. Simple Parameterized Models For Predicting Mobility, Burial and Re-Exposure of Underwater munitions. SERDP Final Report MR-2224. Virginia Institute of Marine Science, William & Mary.
Gao, F.P., Wang, N., Zhao, B., 2013. Ultimate bearing capacity of a pipeline on clayey soils: slip-line field solution and FEM simulation. Ocean Engineering 73, 159–167. https://doi.org/10.1016/j.oceaneng.2013.09.003.
Gourvenec, S., White, D., 2010. Consolidation Around Seabed Pipelines. In: Proceedings of the All Days. Presented at the Offshore Technology Conference. OTC, Houston, Texas, USA. https://doi.org/10.4043/20554-MS p. OTC-20554-MS.
Inman, D.L., Jenkins, S.A., 2002. Scour and Burial of Bottom Mines: a Primer for Fleet Use. Scripps Institution of Oceanography, University of California, San Diego, La Jolla, CA, pp. 02–08.
Jaber, R., Stark, N., Jafari, N., Ravichandran, N., 2021. Combined portable free fall penetrometer and chirp sonar measurements of three texas river sections post hurricane harvey. Eng. Geol. 294, 106324 https://doi.org/10.1016/j.enggeo.2021.106324.
Javankhoshdel, S., Bathurst, R.J., 2014. Simplified probabilistic slope stability design charts for cohesive and cohesive-frictional (c -ϕ) soils. Can. Geotech. J. 51, 1033–1045. https://doi.org/10.1139/cgj-2013-0385.
Jeanjean, P., Spikula, D., Young, A., 2012. Technical Vetting of Free-Fall Cone Penetrometer. Presented at the Offshore Site Investigation and Geotechnics: Integrated Technologies - Present and Future. SUT-OSIG-12-16.
Karlsrud, K., Hernandez-Martinez, F.G., 2013. Strength and deformation properties of Norwegian clays from laboratory tests on high-quality block samples. Can. Geotech. J. 50, 1273–1293. https://doi.org/10.1139/cgj-2013-0298.
Ladd, C.C., Foott, R., 1974. A new design procedure for stability of soft clays. J. Geotech. Eng. Div. ASCE 100, 763–786. NO.GT7.
Li, J., Tian, Y., Cassidy, M.J., 2015. Failure mechanism and bearing capacity of footings buried at various depths in spatially random soil. J. Geotech. Geoenviron. Eng. 141, 04014099 https://doi.org/10.1061/(ASCE)GT.1943-5606.0001219.
Li, X., Hou, Z., Lu, J., Yang, D., He, Z., Cao, Z., Zhao, G., 2021. Research on calculation model of penetration depth when anchor touches Seabed. J. Phys. Conf. Ser., 012015 https://doi.org/10.1088/1742-6596/2006/1/012015, 2006.
Low, B.K., Tang, W.H., 1997. Efficient reliability evaluation using spreadsheet. J. Eng. Mech. 123, 749–752. https://doi.org/10.1061/(ASCE)0733-9399(1997)123:7(749).
Lu, Y., Duan, Z., Zheng, J., Zhang, H., Liu, X., Luo, S., 2020. Offshore cone penetration test and its application in full water-depth geological surveys. IOP Conf. Ser. Earth Environ. Sci. 570, 042008 https://doi.org/10.1088/1755-1315/570/4/042008.
Lunne, T., 2012. The fourth James K. Mitchell Lecture: the CPT in offshore soil investigations - a historic perspective. Geomech. Geoeng. 7, 75–101. https://doi.org/10.1080/17486025.2011.640712.
Mackillop, K., Mitchelmore, P.S., Loewen, N., Jarrett, K., 2016. Geotechnical Data Compilation (1965-2010) and Seabed Characterization of the Outer Shelf and Continental Slope Areas of the Canadian Beaufort Sea. Regional Assessment of Seabed Geohazard Conditions Canadian Beaufort Outer Shelf and Upper Slope: Legacy Data Synthesis.
Medeiros, CJ., 2002. Low cost anchor system for flexible risers in deep water. OTC 14151. Proc. Offshore Tech. Conf.
Mumtaz, M.B., Stark, N., 2020. Pore pressure dissipation induced by high-velocity impacts of a portable free-fall penetrometer in clays. J. Geotech. Geoenviron. Eng. 146, 05020008 https://doi.org/10.1061/(ASCE)GT.1943-5606.0002273.
O'Beirne, C., O'Loughlin, C.D., Wang, D., Gaudin, C., 2015. Capacity of dynamically installed anchors as assessed through field testing and three-dimensional large-deformation finite element analyses. Can. Geotech. J. 52, 548–562. https://doi.org/10.1139/cgj-2014-0209.
O'Loughlin, C.D., Randolph, M.F., Richardson, M., 2004. Experimental and theoretical studies of deep penetrating anchors. In: Proceedings of the All Days. Presented at the Offshore Technology Conference. Houston, Texas. OTC. https://doi.org/10.4043/16841-MS p. OTC-16841-MS.
O'Loughlin, C.D., Richardson, M.D., Randolph, M.F., 2009. Centrifuge tests on dynamically installed anchors. In: Proceedings of the Offshore Geotechnics; Petroleum Technology. Presented at the ASME 2009 28th International Conference on Ocean. Honolulu, Hawaii, USA, 7. Offshore and Arctic Engineering, ASMEDC, pp. 391–399.
Osler, J., Furlong, A., Christian, H., Lamplugh, M., 2006. The integration of the free fall cone penetrometer (FFCPT) with the moving vessel profiler (MVP) for the rapid assessment of seabed characteristics. Int. Hydrogr. Rev. 7. https://journals.lib.unb.ca/index.php/ihr/article/view/20772.
Paniagua, P., L'heureux, J.S., 2019. Comparison of three Norwegian marine clays from a mineralogical, chemical and geotechnical approach. In: Proceedings of the XVII ECSMGE-2019 1410–1417. https://doi.org/10.32075/17ECSMGE-2019-0265.
Paprocki, J., Stark, N., Lippmann, T., 2024. Geotechnical characterization of a tidal estuary mudflat using portable free-fall penetrometers. J. Geotech. Geoenviron. Eng. 150, 04023131 https://doi.org/10.1061/JGGEFK.GTENG-11579.
Rennie, S.E., Brandt, A., Friedrichs, C.T., 2017. Initiation of motion and scour burial of objects underwater. Ocean Eng. 131, 282–294. https://doi.org/10.1016/j.oceaneng.2016.12.029.
Richardson, M.D., O'Loughlin, C.D., Randolph, M.F., Cunningham, T.J., 2006. Drum centrifuge modelling of dynamically penetrating anchors. In: Proceedings of the Sixth International Conference on Physical Modelling in Geotechnics, 6th ICPMG '06. Hong Kong. Taylor & Francis, pp. 673–678. https://www.researchgate.net/publication/279611776_Drum_centrifuge_modelling_of_dynamically_penetrating_anchors.
Robertson, P.K., 2010. Estimating *in-situ* state parameter and friction angle in sandy soils from CPT. In: Proceedings of the 2nd International Symposium on Cone Penetration Testing. Huntington Beach, CA. https://www.cptrobertson.com/PublicationsPDF/Robertson%202010%20Insitu%20State%20CPT10%20cor.pdf.
Sagrilo, L.V.S., Sousa, J.R.M., Lima, E.C.P., Porto, E.C., Fernandes, J.V.V., Foppa, D., 2010. Safety Factor Evaluation For Torpedo Anchors Design. Asociación Argentina de Mecánica Computacional, Buenos Aires, Argentina. https://www.semanticscholar.org/paper/Safety-Factors-Evaluation-for-Torpedo-Anchors-Sagrilo-Sousa/0896d7a93cfd4bbdd0ef700ac4f545bf05d37992.
Shang, Zhao, Zhang, 2019. Obtaining high-resolution seabed topography and surface details by co-registration of side-scan sonar and multibeam echo sounder images. Remote Sens. 11, 1496. https://doi.org/10.3390/rs11121496 (Basel).
Shendi, E.A., 2007. Introduction to Geophysics, 1st ed. Suez Canal University.
Simpson, F., Inderbitzen, A.L., Singh, A., Inderbitzen, A.L., 1974. Initial penetration and settlement of concrete blocks into deep-ocean sediments. Deep-Sea Sediments. Springer US, Boston, MA, pp. 303–326. https://doi.org/10.1007/978-1-4684-2754-7_14.
Sivakumar Babu, G.L., Srivastava, A., 2007. Reliability analysis of allowable pressure on shallow foundation using response surface method. Comput. Geotech. 34, 187–194. https://doi.org/10.1016/j.compgeo.2006.11.002.
Stark, N., Green, B., Brilli, N., Eidam, E., Franke, K.W., Markert, K., 2022. Geotechnical measurements for the investigation and assessment of arctic coastal erosion—a review and outlook. JMSE 10, 914. https://doi.org/10.3390/jmse10070914.
Stark, N., Kopf, A., Hanff, H., Stegmann, S., Wilkens, R., 2009. Geotechnical investigations of sandy seafloors using dynamic penetrometers. OCEANS 2009. Presented at the OCEANS 2009. IEEE, Biloxi, MS, pp. 1–10.
Stark, N., Wilkens, R., Ernstsen, V.B., Lambers-Huesmann, M., Stegmann, S., Kopf, A., 2012. Geotechnical properties of sandy seafloors and the consequences for dynamic penetrometer interpretations: quartz sand versus carbonate sand. Geotech. Geol. Eng. 30, 1–14. https://doi.org/10.1007/s10706-011-9444-7.
Taber, V.L., 1999. Environmental Sensitivity Study of Mine Impact Burial Prediction Model. Naval PostGraduate School, Monterey, California.
Tan, B.B., 2004. Geotechnical Characterization of Sediments from Hydrate Ridge, Cascadia Continental Margin. Massachusetts Institute of Technology, Cambridge.
Terzaghi, K.V., Peck, R.B., Mesri, G., 1996. Soil Mechanics in Engineering Practice, Third. John Wiley & Sons, Inc.
White, D.J., Cathie, D., 2010. Geotechnics For Subsea Pipelines. Frontiers in Offshore Geotechnics II, pp. 87–123.
Wu, L., Cheng, W., Zhu, Z., 2021. Fractional-order elastoplastic modeling of sands considering cyclic mobility. JMSE 9, 354. https://doi.org/10.3390/jmse9040354.
Yang, S.L., Lunne, T., Andersen, K.H., D'lgnazio, M., Yetginer, G., 2019. Undrained shear strength of marine clays based on CPTU data and SHANSEP parameters. In: Proceedings of the XVII ECSMGE-2019, pp. 173–180. https://doi.org/10.32075/17ECSMGE-2019-0048.
Young, C.W., 1997. Penetration equations. OSTI OAI (U.S. Department of Energy Office of Scientific and Technical Information. https://doi.org/10.2172/562498.